

## Report

### Mapping the Silt Content of the Westerschelde Sediments using Satellite Data

<u>Function</u>	<u>Name</u>	<u>Organisation</u>	<u>Signature</u>	<u>Date</u>
Author:	K. Stelzer	BC		19.12.2003

**Title:** Mapping the Silt Content of the  
Westerschelde Sediments using  
Satellite Data

**Project:** SiltCont

**Dok. Name.:** SiltCont\_report\_2.0.doc


**Issue:** 2

**Revision:** 1

**Date:** 19.12.2003


### External Distribution

<u>Name</u>	<u>Organisation</u>	<u>No</u>
Fred Twisk	RIKZ	1
Dirk van Maldegem	RIKZ	1

 <b>BROCKMANN CONSULT</b>	<p>Final Report</p>	<p><b>Doc:</b> SiltCont_report_2.0.doc</p> <p><b>Name:</b> Mapping the Silt Content of the Westerschelde Sediments using Satellite Data</p> <p><b>Date:</b> 19.12.2003</p> <p><b>Issue:</b> 2      <b>Revision:</b>      <b>Page</b> 2</p>
---	---------------------	--

# **Mapping the Silt Content of the Westerschelde Sediments using Satellite Data**

<b>1</b>	<b>Summary .....</b>	<b>3</b>
<b>2</b>	<b>Source Data .....</b>	<b>3</b>
2.1	Landsat 7 ETM .....	3
2.2	Sediment samples .....	3
2.3	Vector file of the coast line .....	3
<b>3</b>	<b>Preprocessing .....</b>	<b>3</b>
3.1	Georeferencing .....	3
3.2	Spatial Subset.....	4
3.3	Sun geometry and atmospheric adjustment .....	5
<b>4</b>	<b>Derivation of Silt Content from Landsat Images .....</b>	<b>7</b>
4.1	Masking of tidal flat areas .....	7
4.2	Analysing of spectral reflectance of different surface types .....	8
4.3	Supervised Classification.....	9
4.3.1	Definition of the training areas.....	9
4.3.2	Results .....	13
4.3.2.1	<i>Classification of the July image .....</i>	<i>13</i>
4.3.2.2	<i>Classification of the February image .....</i>	<i>15</i>
4.3.2.3	<i>Comparison of both images.....</i>	<i>16</i>
4.3.2.4	<i>Comparison with Sample Points .....</i>	<i>16</i>
4.4	Spectral Unmixing .....	17
4.4.1	Method.....	17
4.4.2	Excursus: Comparability sample points and pixels .....	19
4.4.3	Evaluation of the Portion of Dry Mud Endmember.....	21
4.4.3.1	<i>Results July.....</i>	<i>22</i>
4.4.3.2	<i>Results February.....</i>	<i>23</i>
4.4.3.3	<i>Comparison of Silt Content July and February.....</i>	<i>25</i>
4.5	Error Estimation .....	25
4.6	Summary of Results .....	27
<b>5</b>	<b>Conclusion .....</b>	<b>27</b>
<b>6</b>	<b>Terms of Use .....</b>	<b>29</b>
<b>7</b>	<b>Deliverables .....</b>	<b>29</b>
<b>8</b>	<b>Contact .....</b>	<b>29</b>

	<p>Final Report</p>	<p>Doc: SiltCont_report_2.0.doc  Name: Mapping the Silt Content of Westerschelde Sediments using Satellite Data  Date: 19.12.2003  Issue: 2      Revision: <span style="float: right;">Page 3</span></p>
---	---------------------	--

## 1 Summary

The goal of this project is the mapping of the distribution of the silt fraction ( $<63\mu\text{m}$ ) in the tidal flats of the Westerschelde, The Netherlands, by analysing Landsat 7 ETM satellite data. For calibration and verification of the results, an in-situ data set of 300 sediment samples is used. Two different methods are applied and compared in order to retrieve the silt content from the satellite data: a Supervised Classification and a Linear Spectral Unmixing. After the analysis of the satellite data, an error estimation of the results has been performed.

## 2 Source Data

### 2.1 Landsat 7 ETM

Landsat 7 ETM is a spaceborne radiometer, which measures the reflected sun light in 6 spectral bands and 1 pan-chromatic band, as well as the emitted thermal radiance in 1 band. The ground resolution of the data is 30m multispectral and 15m pan-chromatic. Landsat 7 ETM has been optimised for a thematic mapping of land surfaces.

For this study, two satellite scenes from 29.07.2002 and 22.02.2003 have been analysed<sup>1</sup>. The winter scene has the advantage that no vegetation influences the signal, either by totally covering the sediment of the whole pixel, or by partly covering the area of a pixel and thus distorting the spectral measurement. However, a winter scenes suffers from the poor lighting conditions, which lower the spectral signal, especially of dark surfaces such as intertidal flats.

The overpass time of Landsat in this area is approximately 10:30 (GMT). On 29.07.2002 low tide occurred in the Westerschelde at 12:40 local time and on the 22.02.03 at 11:42 local time. Therefore, both scenes have good water conditions for the analysis of the tidal flat areas.

### 2.2 Sediment samples

The silt content (fraction  $<63\mu\text{m}$ ) of the top 5 cm of the sediment of close to 300 samples have been analysed by RIKZ and are made available for this investigation. The samples were collected in summer 2002 on a 500 x 500 m grid.

### 2.3 Vector file of the coast line

An additional data set containing the coast line of the Westerschelde has been provided by RIKZ. This Arc View shapefile was used to gain passpoints for the georeferencing of the satellite scenes as well as for quality check of the georeferencing.

## 3 Preprocessing

### 3.1 Georeferencing

The Landsat scenes had to be georeferenced in order to combine the satellite data with the ground measurements and for further combination with geographical data. The Dutch System RD with Amersfoort Datum has been used as coordinate system. The satellite data is delivered from the provider Eurimage with a spatial accuracy of 250m. However for this investigation, an accuracy of less than 1 pixel ( $<30\text{ m}$ ) is necessary in order to retrieve the best possible correspondence between satellite data and the sediment samples. Therefore a refinement of the georeferencing has been done using reference points which can be clearly detected in both, the satellite data as well as in a reference, e.g. such as a map or digital geolocated data set of the region, with known geolocations. Therefore RIKZ provided a digital data set of the coast line of the Westerschelde.

Figure 1 shows the positions of the 23 passpoints for the July image, which have been selected around the Westerschelde. As a consequence, the georeferencing is only valid for this region. This is reasonable because only the Westerschelde is the area of interest.

---

<sup>1</sup> The satellite images have been ordered and bought by Brockmann Consult at Eurimage (<http://www.eurimage.com>).



*Figure 1: Full satellite scene and passpoints used for georeferencing*

It is important to note that passpoints could only be set on the land areas because fixed points were needed that can be identified in both - the satellite image and the georeferenced data set. Therefore, no passpoints are inside of the tidal flats and no quality check can be performed on the correct position of all tidal flat pixels. This might lead to a slight displacement in some areas and therefore a mismatch of the satellite pixel position and the sample points for some cases.

In a second step, the second Landsat image from February has been georeferenced to the July scene. For this image to image referencing, 35 passpoints, also laying around the Westerschelde, have been used.

### 3.2 Spatial Subset

A bounding box including the investigation area Westerschelde with the coordinates in Figure 2 has been used to cut this area out of the whole satellite scenes. All further analyses were performed with these spatial subsets.

*Table 1: Coordinates of the spatial subset showing the investigation area, projection Dutch RD*

	X-Coordinate	Y-Coordinate
Upper left corner	28499.323	388700.968
Lower right corner	75569.323	370730.968




	<p>Final Report</p>	<p>Doc: SiltCont_report_2.0.doc  Name: Mapping the Silt Content of Westerschelde Sediments using Satellite Data  Date: 19.12.2003  Issue: 1      Revision: <span style="float: right;">Page 5</span></p>
---	---------------------	--



Figure 2: Investigation area overlaid with border and sampling points provided by RIKZ (July image)

### 3.3 Sun geometry and atmospheric adjustment

The satellite is measuring spectral radiances,  $L(\lambda)$ , which are very different for the two scenes because of the much lower sun elevation in winter time, expressed as higher sun zenith angle  $\Theta_s$ . By converting the radiance into reflectances,  $r_{sat}(\lambda)$ , this effect is removed:

$$r_{sat}(\lambda) = \frac{L(\lambda) \cdot \pi}{E_0(\lambda) \cdot \cos(\theta_{sun})} \quad [F 1]$$

$E_0(\lambda)$  is the solar irradiance.

An important contribution to the measured reflectance at the satellite are the reflectance and the transmission of the atmosphere. These have to be removed in order to retrieve the portion of the signal which is relevant for this study, namely the reflectance of the surface, and also in order to make the two scenes comparable, which is not possible without correction because of the varying atmospheric conditions. This is a major prerequisite for the application of the Linear Spectral Unmixing method.

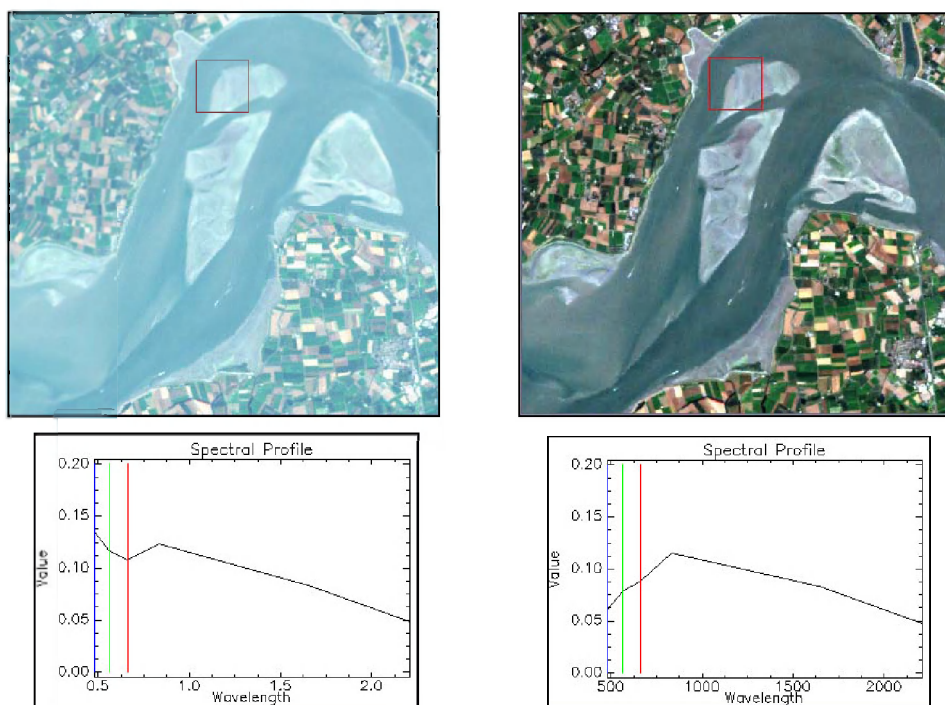
The effect of the atmosphere can be separated into the reflectance caused by scattering of air molecules, so called Rayleigh scattering,  $r_{Rayl}(\lambda)$ , and the one of aerosol particles. While the Rayleigh scattering can be removed without additional auxiliary data, the aerosol scattering requires knowledge of the aerosol type and concentration at the moment of the measurement. The aerosol reflectance is in short wavelength bands much lower than the Rayleigh reflectance and can be neglected as a first, simple approximation.

The Rayleigh reflectance has a strong wavelength dependence and has to be subtracted from each band individually. The sun and viewing angles ( $\Theta_s$  and  $\Theta_v$ ) are also important for the strength of the Rayleigh scattering. For example, a lower sun results in a longer path of the light from the sun to earth and therefore more interaction with air molecules, resulting in higher scattering. However, these dependencies are well understood and can easily be modelled.

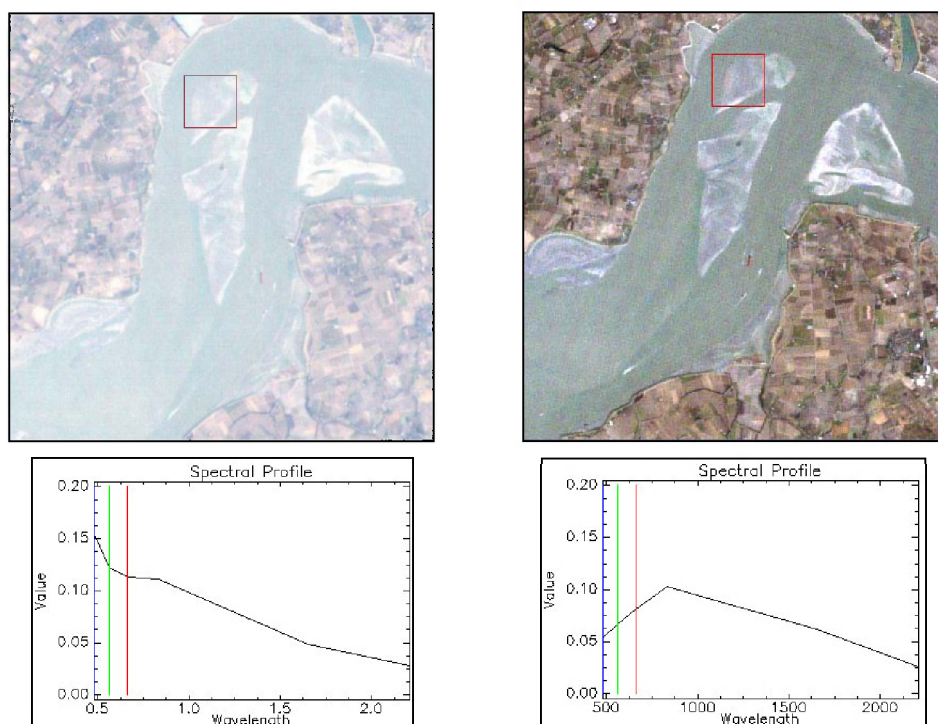
$$r_{surf}(\lambda) = r_{sat}(\lambda) - r_{Rayl}(\lambda, \theta_s, \theta_v) \quad [F 2]$$

$$r_{Rayl}(\lambda) \sim \lambda^{-4} \quad [F 3]$$

Figure 3 and Figure 4 show the influence of the Rayleigh reflectance in the visualisation of the images as well as in the surface reflectances.



*Figure 3: Influence of the atmosphere on the image and the reflectance spectra (July image)*



*Figure 4: Influence of the atmosphere on the image and the reflectance spectra (February image)*

After subtracting the Rayleigh reflectance from both images, the spectra of the same pixels look similar, thus similar endmember sets for the spectral unmixing method can be used for getting comparable results (see section 4.4).

## 4 Derivation of Silt Content from Landsat Images

The final goal of this project is to produce a map of the silt content in the tidal flats of the Westerschelde. After the atmospheric and geometric correction, the next step is to produce a mask of the tidal flats in the images. This is used to restrict all subsequent analyses only to the tidal flat areas. For the critical step of the classification of these areas into silt content classes, two methods have been used: a Supervised Maximum-Likelihood Classification and the Spectral Unmixing Analysis. While the first method provides discrete classes of different surface types, the latter offers the percentage of silt in each pixel.

### 4.1 Masking of tidal flat areas

Tidal flats have been masked so that the analyses concentrates only on the surfaces of interest. For the masking, a coarse unsupervised classification has been performed, with which the land surfaces could be separated from water and tidal flats. A second unsupervised classification on these areas enabled to discriminate water and sediment surfaces very well. The ships that can be seen on the satellite image were classified as sediment as well, these spots were erased by hand from the mask. Figure 5 shows the remaining intertidal flat areas, this data set is the input for all further analyses. In the following, the tidal flats bordering the dykes are named "Slik" and tidal flats surrounded by water are named "Plate" in correspondence to the Dutch naming of the single tidal flats.

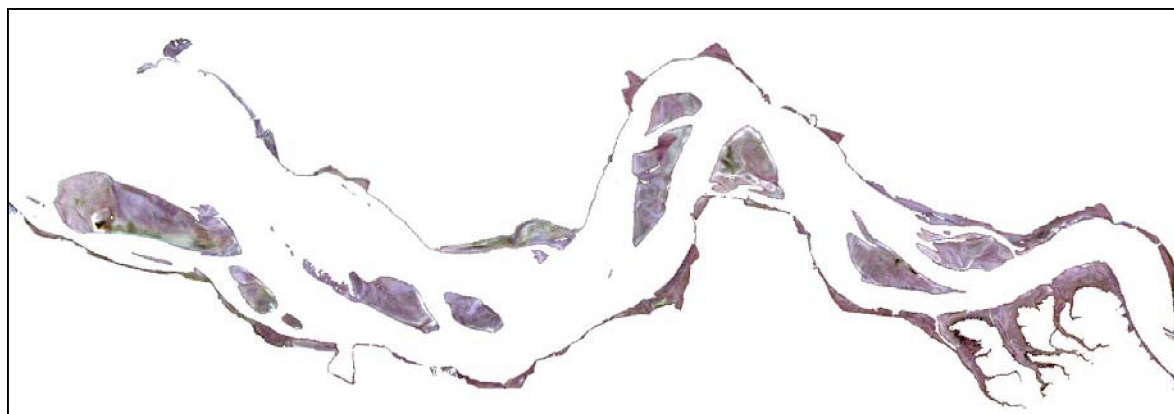


Figure 5: Masked Sediment areas of the Westerschelde, July

After applying the mask, 35 of the in-situ sample points lay outside of the mask because of water coverage of the sediment or dense vegetation coverage during the time of the satellite overpass. 295 samples are left from which 290 remain when the NODATA in-situ samples are subtracted from this set.

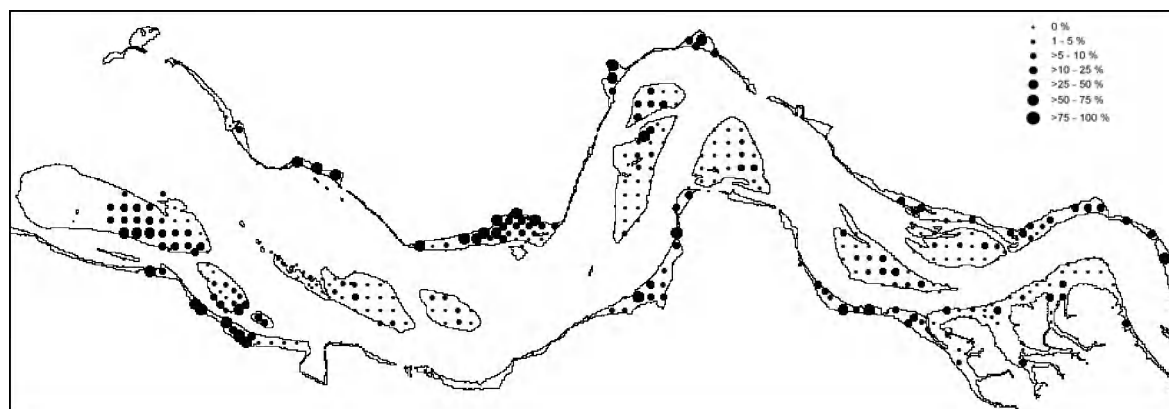



Figure 6: Locations of in-situ measurements, the symbol size is showing the silt content at the points



	<p>Final Report</p>	<p>Doc: SiltCont_report_2.0.doc  Name: Mapping the Silt Content of Westerschelde Sediments using Satellite Data  Date: 19.12.2003  Issue: 1      Revision: <span style="float: right;">Page 8</span></p>
---	---------------------	--

## 4.2 Analysing of spectral reflectance of different surface types

Important surfaces of intertidal flats are sediment (sand, mud), algae (macro and micro) and water. The signal of the sediment is influenced by several factors: sand has a high reflection over all bands (see Figure 16) while muddy sediments are darker because their reflection is less than the one of sand. When water remains on the sediment, it reduces the signal in all band, but especially in the near infrared (bands 4, 5 and 6). This means that the sediment type can be still detected even if parts are under water, because the sand is still brighter in the visible bands. However, the possibility of discrimination of the sediment type decreases with increasing water coverage and beyond a certain point of water coverage no proper discrimination can be performed any more. If the sediment is totally covered by water, the reflectance in band 5 and 6 is almost 0, because of the high absorption of water in these wavelengths.

In addition, the intertidal flat sediment is often covered by vegetation such as sea grass, macro or micro algae. Vegetation has a very high reflection in the near Infrared and an absorption peak in the visible red. If the coverage of vegetation too dense, it also becomes difficult to determine the sediment type.

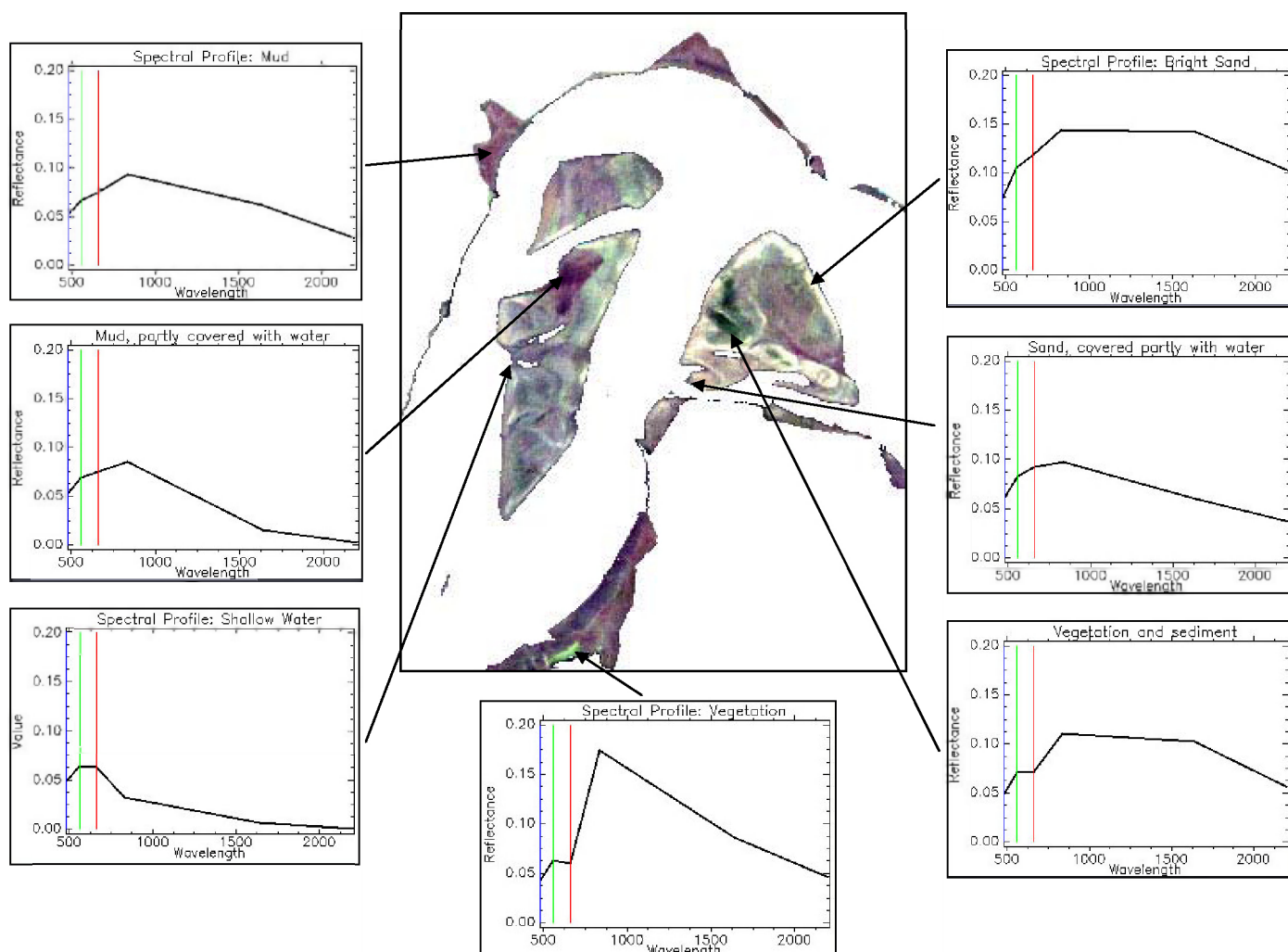



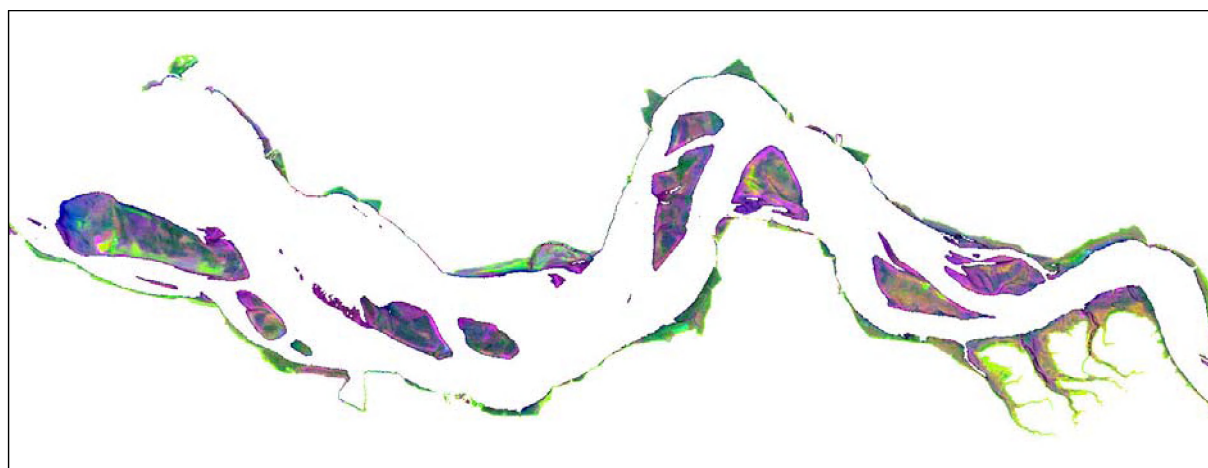
Figure 7: Spectral reflectance of different surface types

The visualization of the satellite image is reduced to 3 bands at once, which means that the information of the other bands can not be seen. In order to reduce the number of bands while



	<p>Final Report</p>	<p>Doc: SiltCont_report_2.0.doc  Name: Mapping the Silt Content of Westerschelde Sediments using Satellite Data  Date: 19.12.2003  Issue: 1      Revision: <span style="float: right;">Page 9</span></p>
---	---------------------	--

preserving most of the information of all bands, 3 indices have been calculated. Water information can be derived from bands 5 or 6 as it reduces the signal very strongly in the near Infrared. The sediment type correlates with the brightness of the visible (and near Infrared) bands. Vegetation can be well detected by an vegetation index that uses bands 3 and 4. The resulting 3-band image can be seen in Figure 8, which shows much more information. The colours can be roughly explained as follows: blue: shallow water, pink: dry sands, violet: water covered sands, dark green: muddy sediment, light green: vegetation



*Figure 8: 3-band image from 'visible brightness', vegetations index, water index; blue: shallow water, pink: dry sands, violet: water covered sands, dark green: muddy sediment, light green: vegetation*

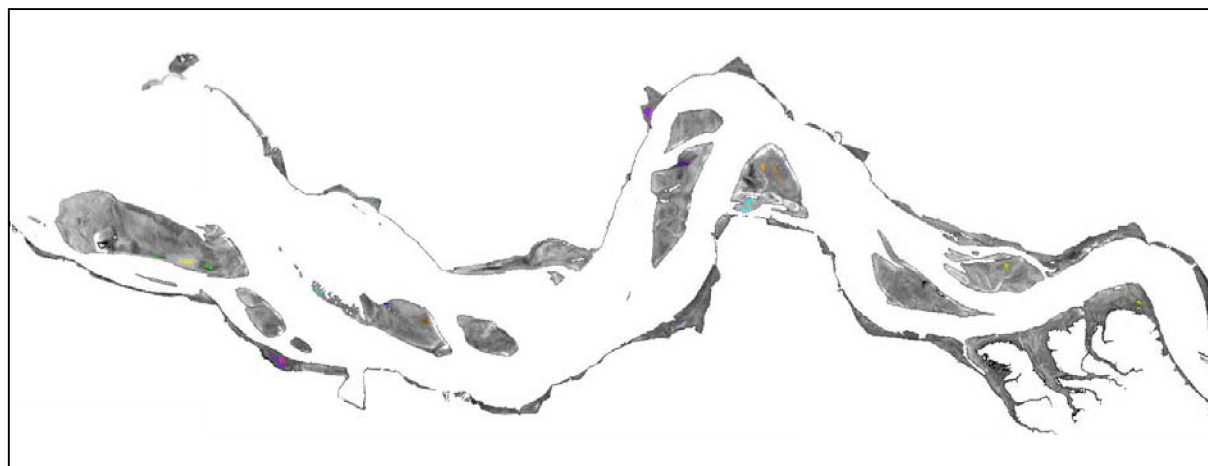
This composite has also been used for understanding the behaviour of the reflectances of the different surface types and for defining the training areas and finding spectra of pure sediment types for the following analyses (see scatter plots Figure 10).

### 4.3 Supervised Classification

#### 4.3.1 Definition of the training areas

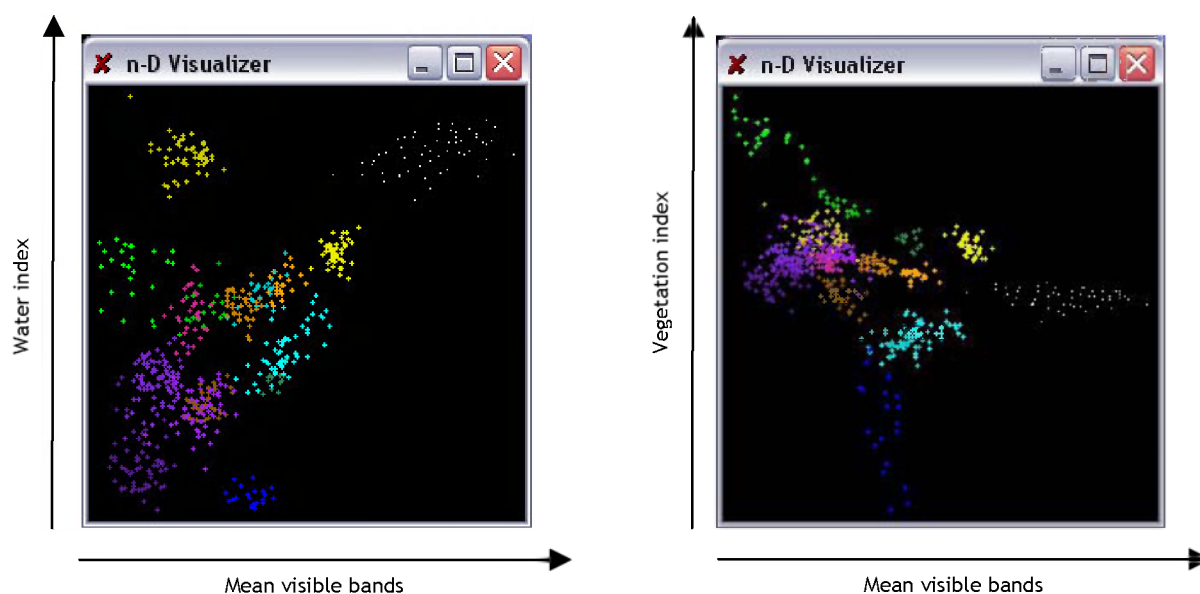
A supervised classification uses predefined training areas of homogenous, known surfaces. These training areas provide the statistical basis which will be used to assign each pixel of the image to one of the pre-defined classes. The quality of the classification depends strongly on the quality of the training set.

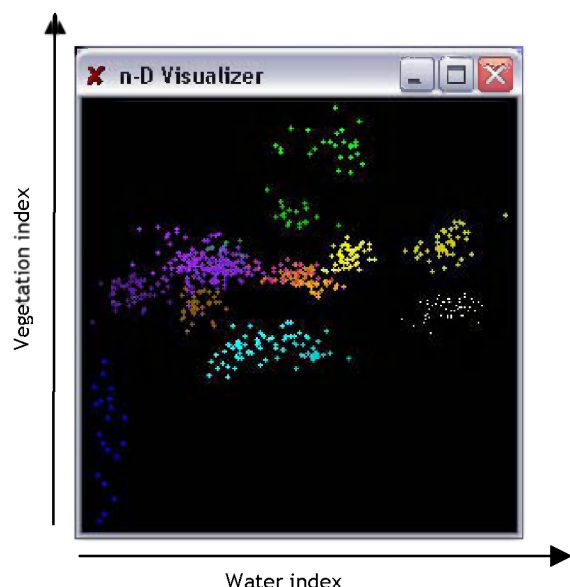
The definition of the training areas has been done mainly with the 3-band index image (Figure 8). The in-situ sample points as well as the spectral reflectance have been taken into account for defining the surface type of each training area. However the training areas are not defined at the exact positions of the in-situ samples due to the bad correlation of in-situ measurements and satellite image, which will be discussed later. Figure 9 shows the positions of the training areas. In order to define homogeneous surface types, those areas are rather small (class names for different colours see legend of Figure 11).



*Figure 9: Positions of Training areas*

The position of the training areas in the data space built by the 3 index bands is shown in Figure 10. The different colours correspond to the different classes (class names for different colours see legend of Figure 11). During the Maximum-Likelihood classification, the mean and standard deviation of each class is calculated and used for the assignment of all pixels. It is important that the different classes do not overlap and that most of the data space is covered by a cluster.





*Figure 10: Position and variance of the training areas used for the supervised classification, see class names below*

Some surfaces (classes) can be clearly separated from others (e.g. the bright green points, which represent dry sediment covered with vegetation). However especially the different mixed sediment and mud classes lay near by each other (orange and purple points). The latter means that there are no clear boundaries but a gradual transition from one class to the other. While the boundary between mixed and muddy sediments are more fluent, the sandy areas, especially of bright sand can be discriminated quite clearly (white and yellow points).

It is possible to calculate the separability between the classes on the basis of the statistics of the training areas. ENVI software uses the Jeffries-Matusita and Transformed Divergence separability. The values range from 0 to 2.0 and indicate how well the selected pairs of training areas are statistically separate. Values greater than 1.9 indicate that the training areas have good separability. For pairs with lower separability values, it should be attempt to improve the separability by editing the training areas. For pairs of training areas with very low separability values (less than 1), they might be combined into a single ROI. Table 2 shows the values for separability derived from the Jeffries-Matusita method. Most of the classes can be separated quite well. In order to consider the classes with less separability, a second trainings set with merged classes has also been applied.




	<p>Final Report</p>	<p>Doc: SiltCont_report_2.0.doc</p> <p>Name: Mapping the Silt Content of Westerschelde Sediments using Satellite Data</p> <p>Date: 19.12.2003</p> <p>Issue: 2      Revision:      Page 12</p>
---	---------------------	---

Table 2: Separability of training areas (Jeffries-Matusita method); good separability: 2.00, medium separability: up to 1.9, no separability: < 1.0

	Sand I (veg dense 1)	Sand II (veg dense 1)	Sand partly covered with water I	Sand partly covered with water II	Mixed Sediment I (sandy)	Mixed Sediment II	Mixed Sediment III (water)	Mixed Sediment IV (Veg)	Mud I (dry)	Mud II	Mud III (water)	Mud covered with water*	Shallow Water	Dry Sediment covered with Veg I	Dry Sediment covered with Veg II
Bright Sand	2.00	2.00	2.00	2.00	2.00	2.00	2.00	2.00	2.00	2.00	2.00	2.00	2.00	2.00	2.00
Sand I (vegetation dense 1)		2.00	2.00	2.00	2.00	2.00	2.00	2.00	2.00	2.00	2.00	2.00	2.00	2.00	2.00
Sand II (vegetation dense 1)			2.00	2.00	2.00	2.00	2.00	2.00	2.00	2.00	2.00	2.00	2.00	2.00	2.00
Sand partly covered with water I				1.98	2.00	2.00	1.99	2.00	2.00	2.00	2.00	2.00	2.00	2.00	2.00
Sand partly covered with water II					2.00	2.00	2.00	2.00	2.00	2.00	2.00	2.00	2.00	2.00	2.00
Mixed Sediment I (sandy)						1.87	2.00	2.00	2.00	2.00	2.00	2.00	2.00	2.00	2.00
Mixed Sediment II							2.00	2.00	1.93	1.99	2.00	2.00	2.00	2.00	2.00
Mixed Sediment III (water)								2.00	1.99	1.86	1.93	1.98	2.00	2.00	2.00
Mixed Sediment IV (Vegetation)									2.00	2.00	2.00	2.00	2.00	2.00	2.00
Mud I (dry)										1.95	1.72	2.00	2.00	2.00	2.00
Mud II											1.83	1.96	2.00	2.00	2.00
Mud III (water)												1.77	2.00	2.00	2.00
Mud covered with water*													2.00	2.00	2.00
Shallow Water														2.00	2.00
Dry Sediment covered with Vegetation I															1.99

#### 4.3.2 Results

The following figures show the results of the supervised classification. Two different sets of training areas were used: one containing 16 classes and another one with 11 classes, which have been derived by merging training areas from the first set. The same training areas have been used for both images, however for the February image, slight changes have been made. One class has been added, as there is a large area of water covered mixed sediments (Hooe Platen). In addition, the number of vegetation classes has been reduced due to less appearance of vegetation in February.

##### 4.3.2.1 Classification of the July image

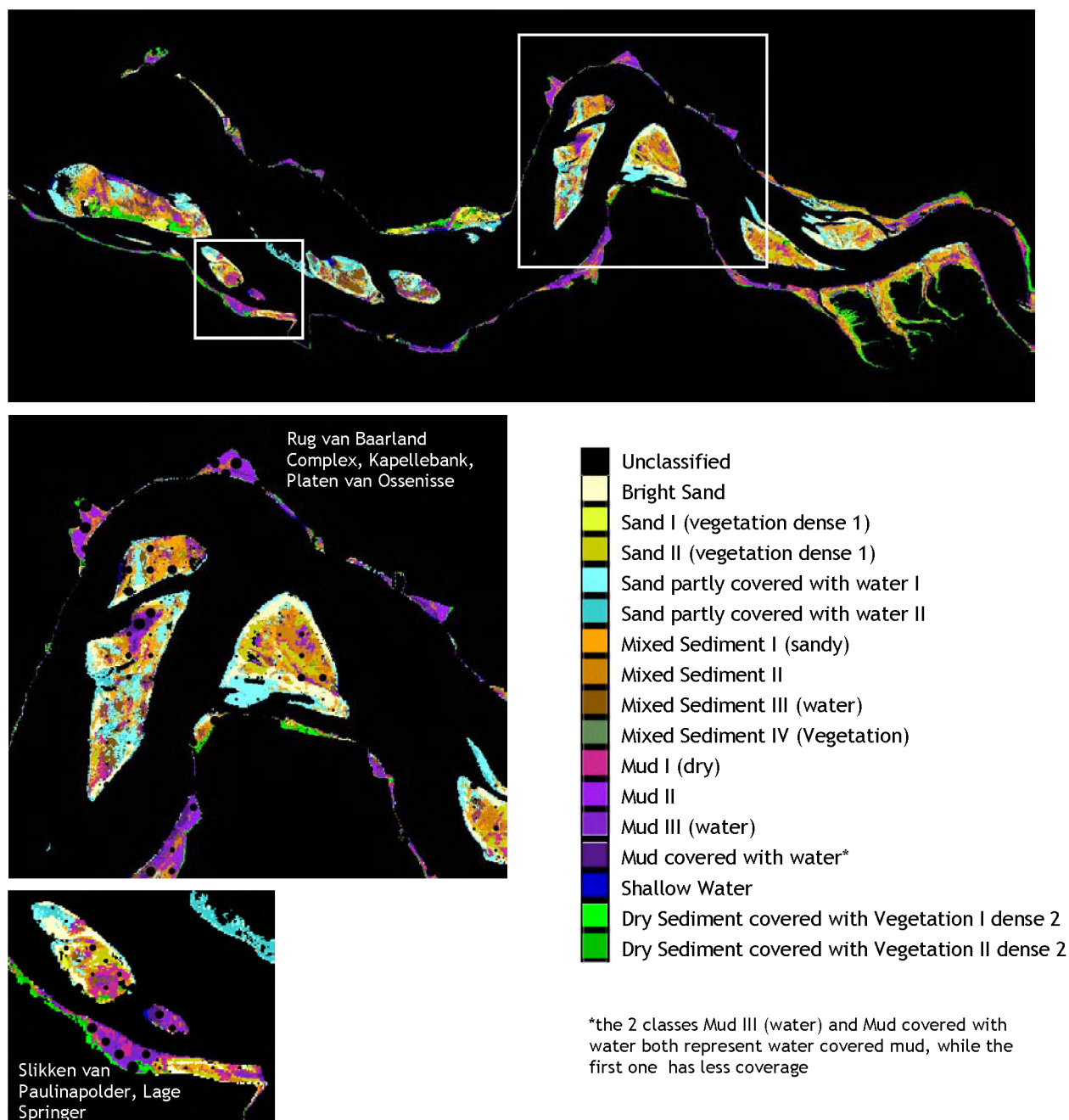
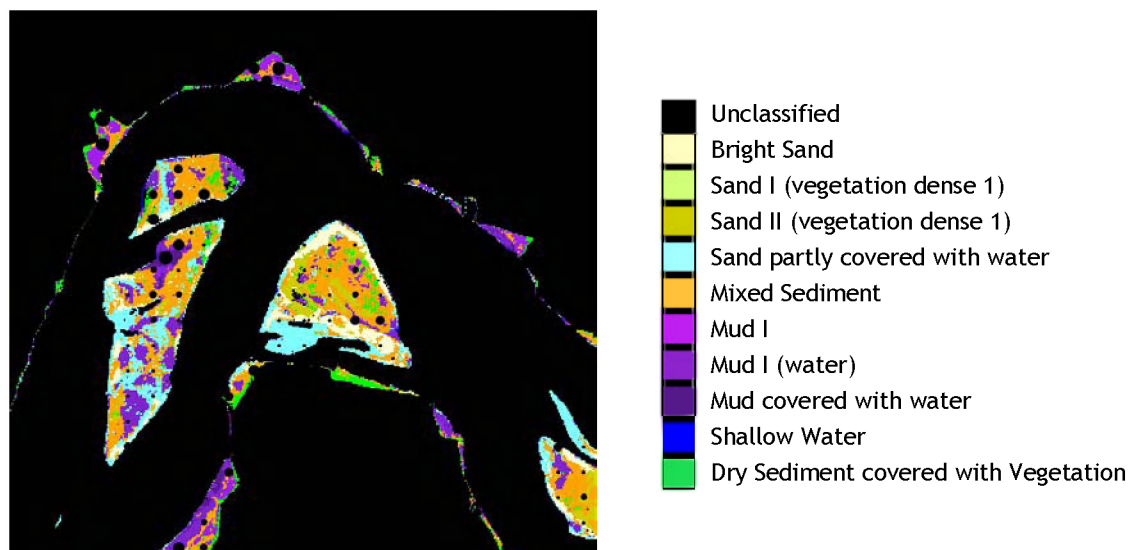


Figure 11: Supervised classification of the July Image; below: subsets overlaid with sample points.



*Figure 12: Supervised classification of the July image; merged classes*

The classification result from July shows in both training sets the trend from muddier areas at the coast to more sandy areas within the Westerschelde. In the subsets of Figure 11 it can be seen that in some areas, the agreement of classification and in-situ measurements is very good (e.g. Slikken van Paulinapolder and east part of Lage Springer). But in other cases, the classification and in-situ measurements do not correspond (western part of Lage Springer). This aspect, that the general trend of satellite data and in-situ measurement is the same, but not necessarily in each single point will be discussed later (section 4.4.2).



#### 4.3.2.2 Classification of the February image

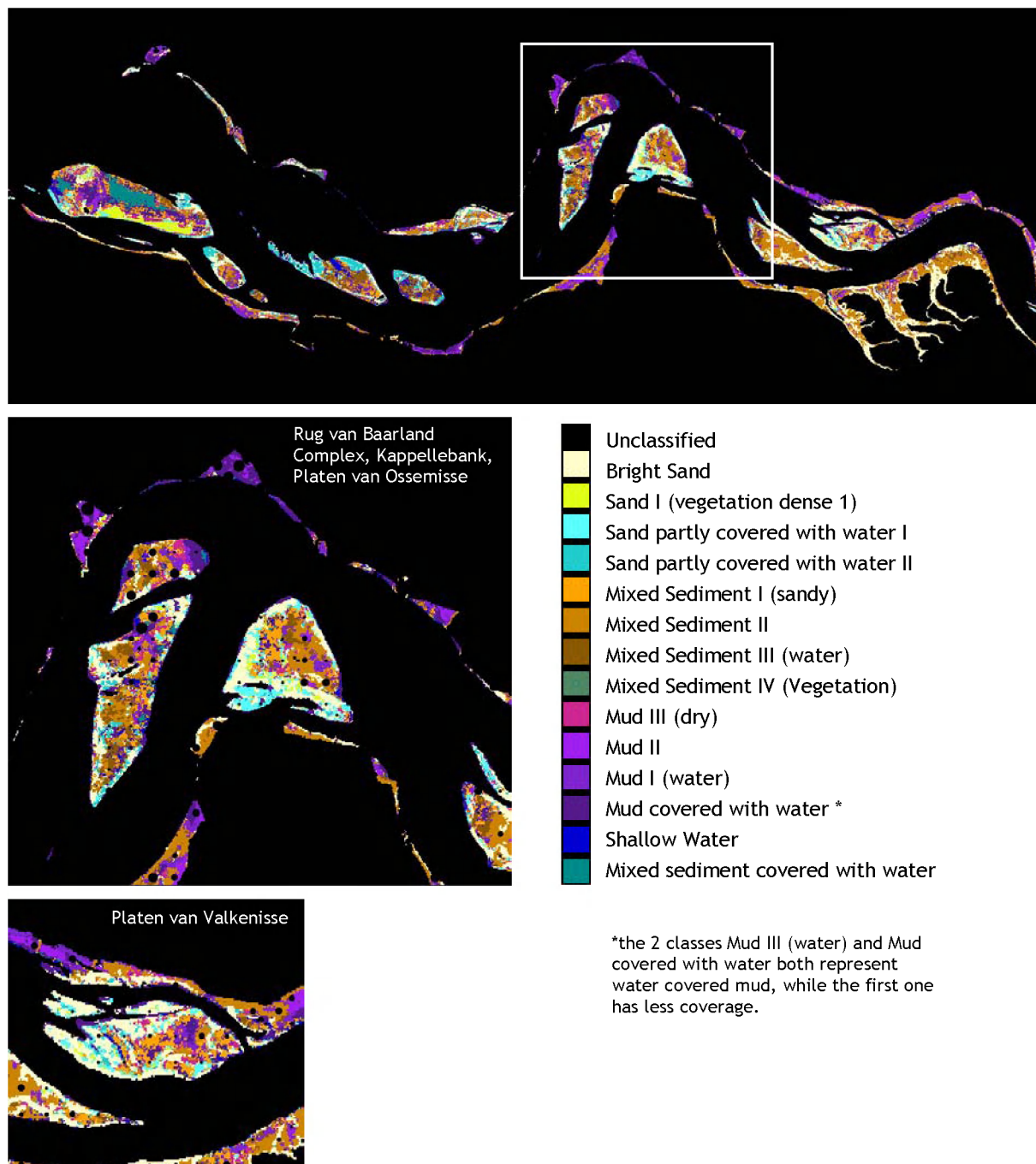


Figure 13: Supervised Classification of the February image; below: subset overlaid with sample points

Also the February image shows the tendency of muddier areas at the coast and areas where the classification fits to the in-situ measurements. The Platen van Valkenisse e.g. is classified as sand in the western part and becoming muddier to in the central eastern part. But again, this is a tendency where agreement can be seen, but when analysing the pixel at the location of the points, this the agreement is not detectable.

### 4.3.2.3 Comparison of both images

Both images (July and February) show the same tendency as the sample points with more sandy sediments in the central region of the Westerschelde (Platen) and muddier sediment on the mudflats bordering the coast (Slikken). In July, the sediment is often covered by vegetation, while the February image shows much more bare sediment surfaces, which are mainly sandy or mixed sediments.

Figure 14 shows the histograms of the classes for the February and July classifications (merged trainings set). It can be seen that in February more pixels were classified as bright sand, which is caused by the splitting of this class into sand & vegetation and water covered sand in the July image.

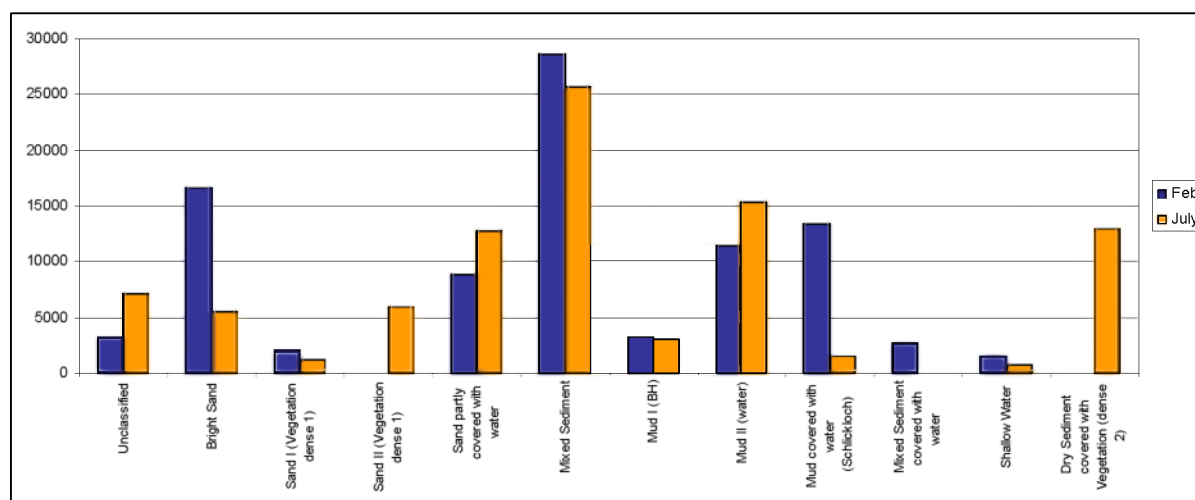


Figure 14: Histogram of classes comparing February and July (merged set of classes)

### 4.3.2.4 Comparison with Sample Points

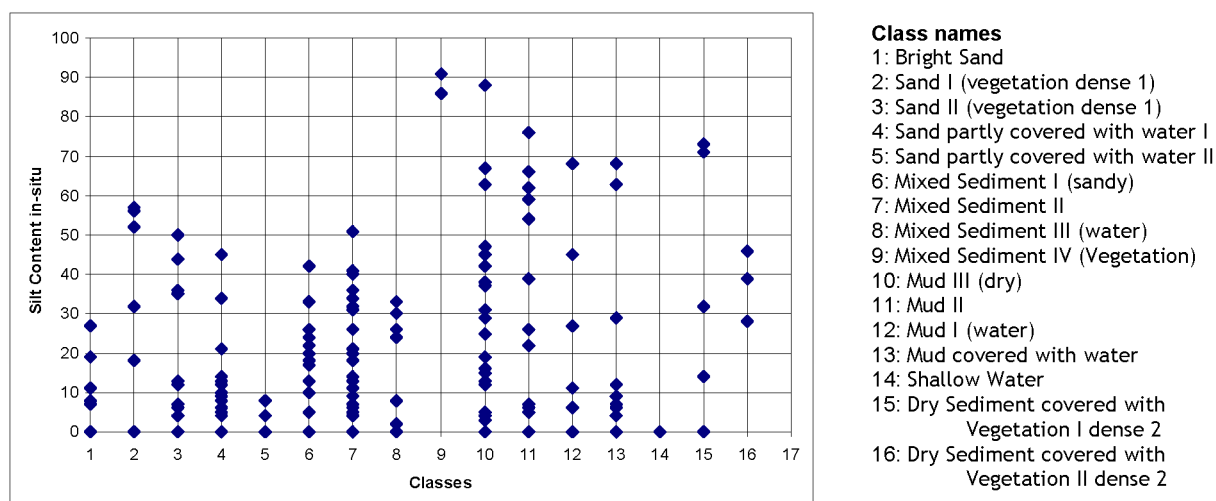



Figure 15: Silt content of in-situ measurements in the different classes

Figure 15 shows the silt content of the in-situ measurements that compared to the classes derived from the satellite image. It confirms what has been previously stated. Only a very slight trend can be seen for the mud classes to contain more sample points with more silt content and the direct comparison of sample points and satellite pixel does not seem possible. A discussion about the comparability can be found in section 4.4.2.

 <b>BROCKMANN CONSULT</b>	Final Report	<b>Doc:</b> SiltCont_report_2.0.doc <b>Name:</b> Mapping the Silt Content of Westerschelde Sediments using Satellite Data <b>Date:</b> 19.12.2003 <b>Issue:</b> 1 <b>Revision:</b> <span style="float: right;">Page 17</span>
---	--------------	--

## 4.4 Spectral Unmixing

### 4.4.1 Method

The reflectance in each pixel is a combination of all surface types which occur on the surface in an area of 30 x 30 meters. The Spectral Unmixing method analyses the sub-pixel percentage (portion) of surface types within each pixel. The satellite data are unmixed by using so-called “endmember spectra”, which is the spectral signature of pure surface types. The percentage of each endmember surface will be calculated for each pixel, and can be expressed as follows:

$$R = a \cdot R_{EM1} + b \cdot R_{EM2} + \dots + n \cdot R_{EMn} + \varepsilon \quad [F\ 4]$$

where

R = Reflectance in the Pixel  
a, b, ..., n = Portions of single Endmembers  
R<sub>EM</sub> = Reflectance of Endmember  
ε = Error of Estimation (RMS)

The endmembers were taken from the satellite data, the choice of the endmembers is the critical factor for the spectral unmixing. The endmember set should contain the most important surfaces that appear in the region. However the number of endmembers is limited due to the mathematics (maximum number of endmember is the same as the number of bands) and they are even more limited in intertidal flat areas which are relatively dark and reflect only a small part of the incoming light. This is why the variability is small and hence a discrimination of surface types is more difficult than over land.

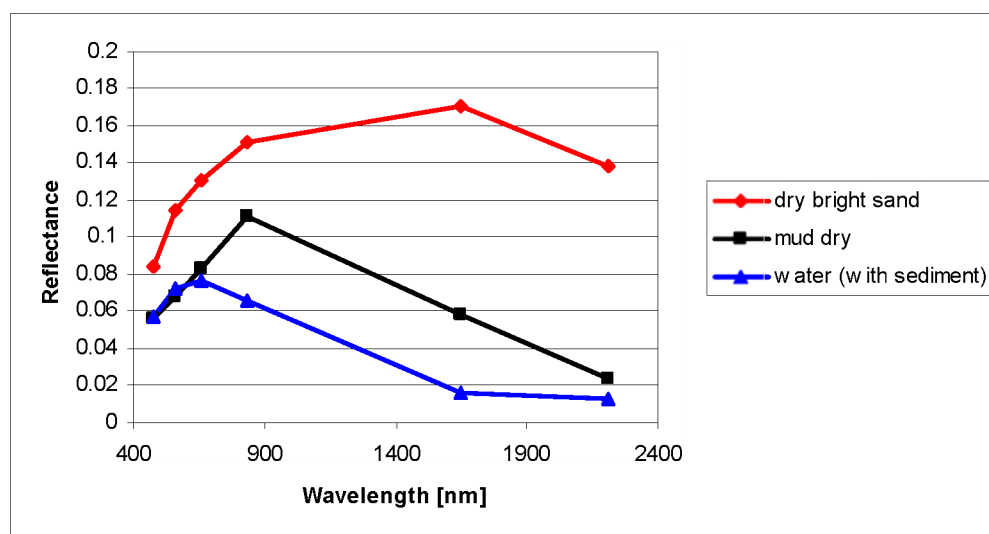



Figure 16: Spectra taken as Endmember for the spectral unmixing

The best results for the unmixing could be retrieved with a 3-endmember set having 2 sediment endmembers and 1 water endmember. The sediment endmember are from “dry” sediment surfaces which means that there is little or no water coverage on the sediment. The water endmember is a mixture of water and sediment.

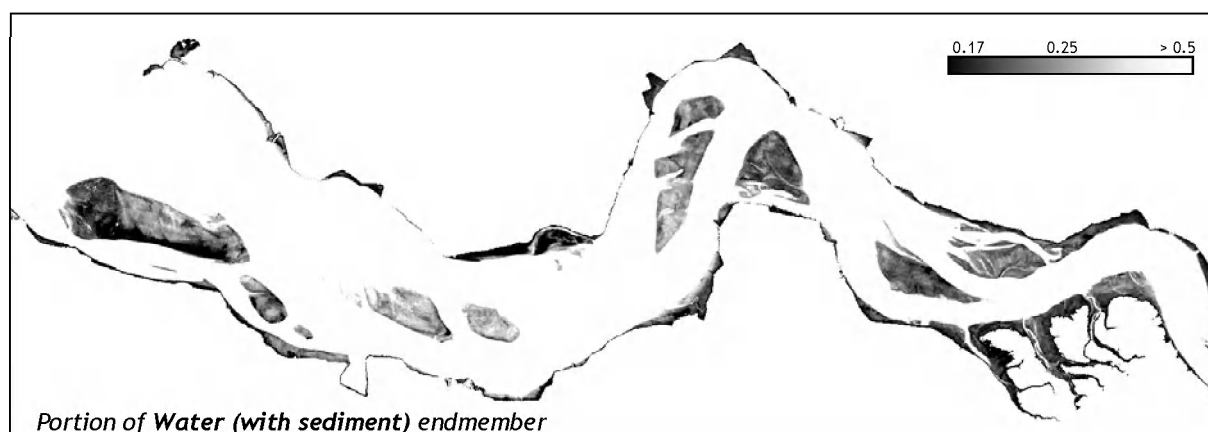
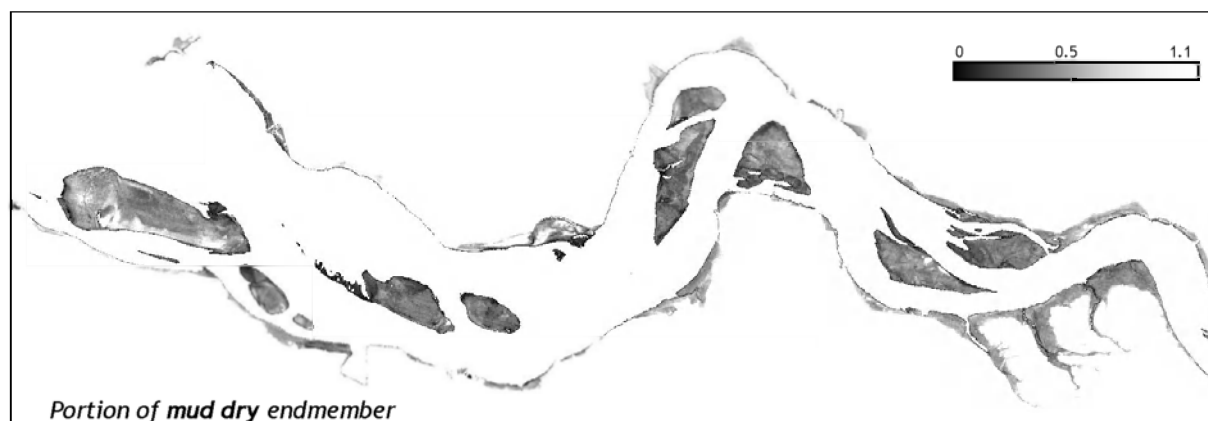
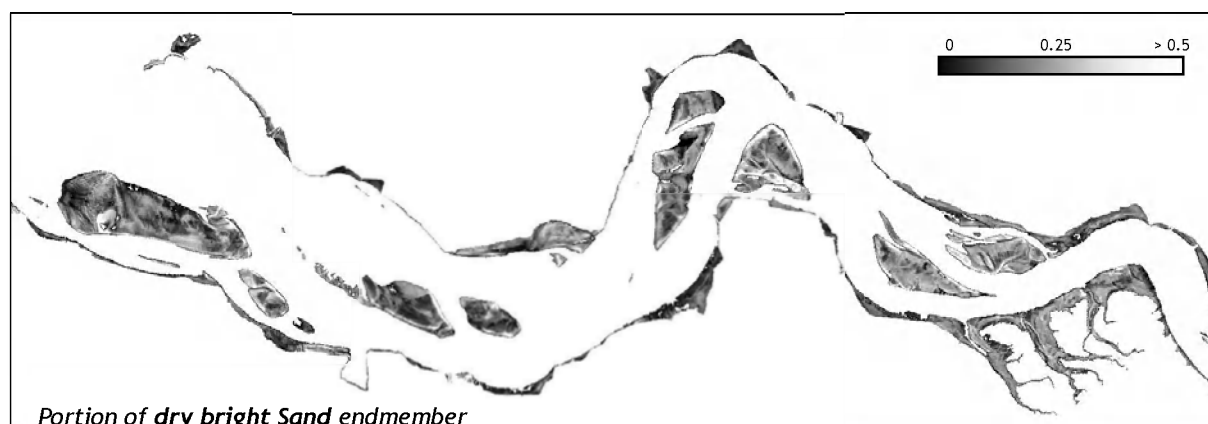
Because of the above described restrictions on the number of endmembers, the maximum number of endmember spectra is 3 for intertidal flats, so that no vegetation endmember is included in this endmember set. The unmixing method also calculates an RMS error, which indicates how good the calculated combination of the given endmember reconstructs the values of the pixels. In this case, a high RMS error correlates very highly with the vegetation covered areas. Therefore an indirect detection of dense vegetation is possible. In this investigation, these areas were not considered in



	<p>Final Report</p>	<p>Doc: SiltCont_report_2.0.doc  Name: Mapping the Silt Content of Westerschelde Sediments using Satellite Data  Date: 19.12.2003  Issue: 1      Revision: <span style="float: right;">Page 18</span></p>
---	---------------------	---

the further analyses, because the information about the sediment type is too difficult to determine under dense vegetation.

The following images show the portions of the 3 endmembers. The pixel values are the coefficients expressed in the above equation. A value of 0 indicates that the pixel does not contain this surface type represented by the endmember, while a value of 1 indicates, that the pixel contains 100% of the surface represented by the endmember. The portion image of the sand endmember and the mud endmember show opposite structures with high values in the sand portion and low values in the mud portion and vice versa. However, the third portion image, derived from the water endmember, indicates where water covers the sediment. Usually, the water portion is influenced by the topography of the tidal flats, the exposure time of the tidal flat and the sediment. The forth image shows the RMS error of this unmixing result. It indicates how well the reflectance of a pixel could be simulated by the used endmember set.



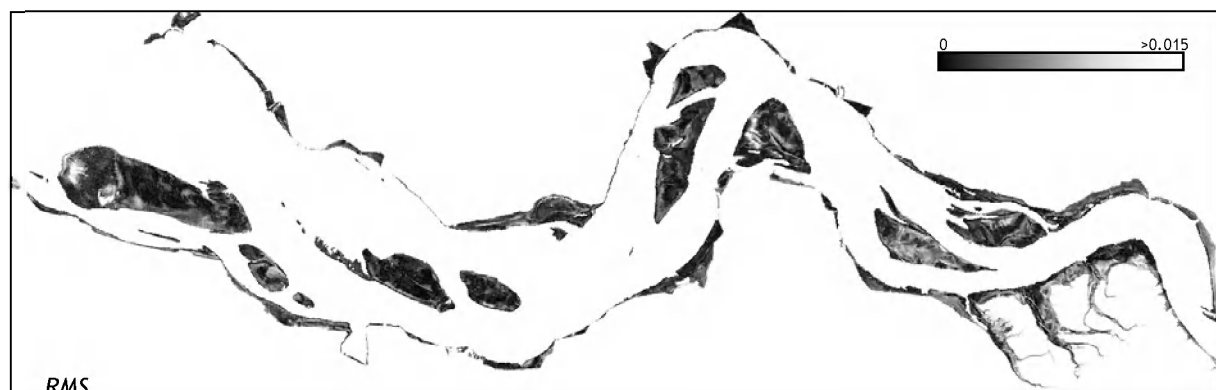


Figure 17: Output of the linear unmixing method: 1 image for each endmember with the portion of each endmember and the error for each pixel.

From these portion images, the one of the dry mud endmember is the most important for this investigation. Since the water coverage is not of interest in this case, it will be subtracted from the portions of sand and mud so that the relation of the both sediment portions is left. The corrected mud portion and respectively the corrected sand portion are calculated by the following equation.

$$port_{mudcorr} = port_{mud} + \frac{port_{mud}}{port_{mud} + port_{sand}} * port_{water} \quad [F 5]$$

As mentioned before, the RMS error that has been calculated for each pixel is high if the endmember set is not optimal for the pixel. In this case, high RMS values correlate with high vegetation coverage. Now it is possible to visualize the 2 sediment endmember portions with the RMS error and retrieve a colour composition image that shows sands in red, mud in blue and vegetation in cyan and green (Figure 18). The colours indicate the relative portion of the sediment endmembers, please note, that this gives the percentage of the endmember of each pixel, which is not identical with the silt content.

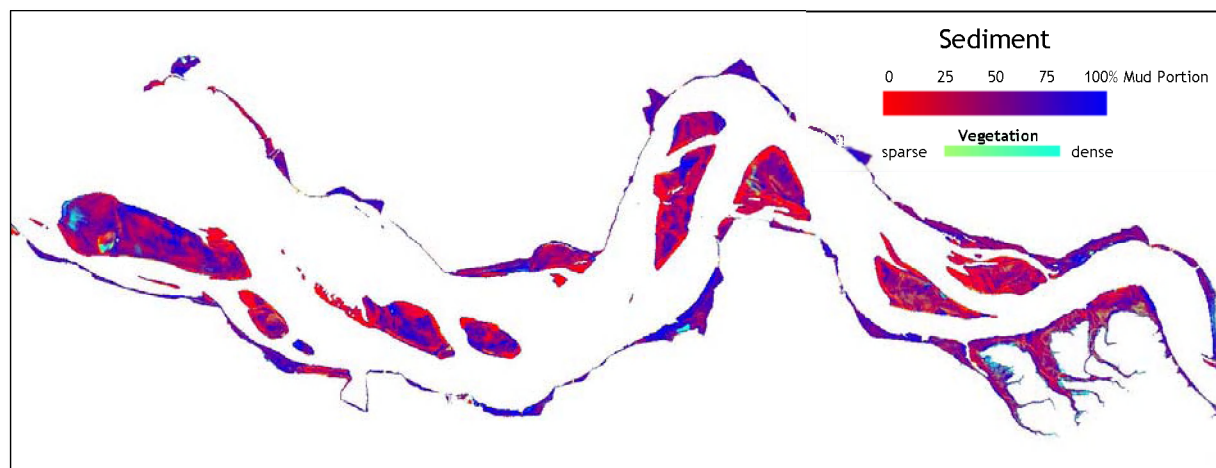


Figure 18: Colour composite from water corrected sand portion, water corrected mud portion and "vegetation" (high RMS values)

#### 4.4.2 Excursus: Comparability sample points and pixels

All data sets, namely the in-situ samples, the classification and the Unmixing of the two satellite images, show the same tendency.

The first guess was to compare the mud content at the exact pixel position of the sample points. As this did not lead to a reasonable result, it has been investigated why this was so and how we were to proceed.

When working with remote sensing data it is always a discussion on how they fit to in situ measurements and how comparable are both methods. It must to be taken into account that one is comparing 2 very different methods and results.

When comparing remote sensing data and in-situ data, it has to be taken into account that optical satellite data only detects the first few nm of the surface while the sediment samples average the upper 5 cm. Especially during calm weather conditions and slow currents, a thin silt layer can be deposited on sandy areas. These areas will be classified as silt in the satellite data whereas they are actually sandy in the sediment samples. This aspect has been investigated by a working group of GKSS. Samples have been taken at different intertidal habitats of 5 cm depths and of 1mm depths in direct neighbourhood and different parameters have been measured for both sample depths. Figure 19 shows that there is a correlation of mud content between the different sample depths. The trend is the same in both sample depths: low mud content in 5 cm depths also has a low mud content in the first mm of the surface and vice versa. However it can also be seen, that there can be a scatter of points and when looking at the differences between 5cm and 1mm samples it can differ +/- 20 % mud content.

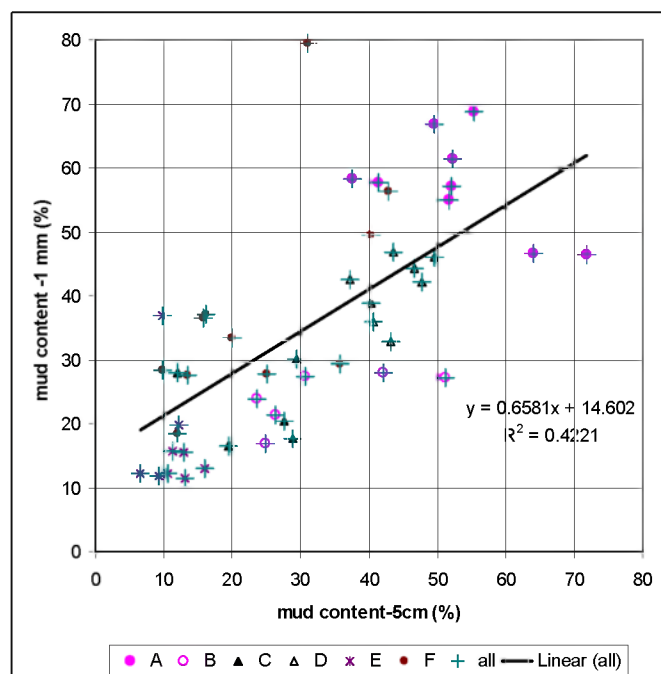


Figure 19: Correlation of mud content between 5 cm deep samples and 1mm deep samples<sup>2</sup>(the samples are taken in different habitats (A-F))

<sup>2</sup> Mahatma, L., Riethmueller, R., van Bernem, K.-H., Andersen, T. (GKSS publication, in prep.) The influence of macrobenthic assemblages on the large scale pattern of sediment surface stability on an intertidal mudflat in the East Frisian Wadden Sea



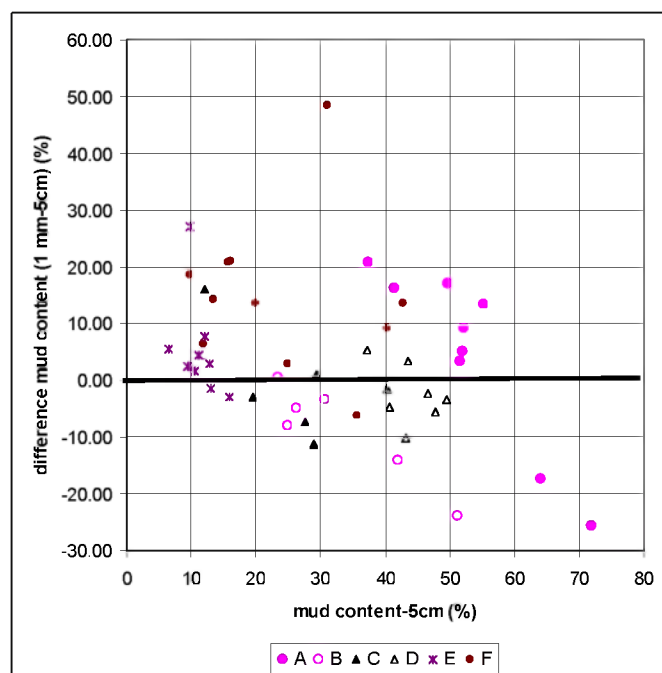


Figure 20: Differences of mud content in 5cm samples and 1mm samples in relation to the mud content in 5cm samples<sup>2</sup> (the samples are collected in different habitats (A-F))

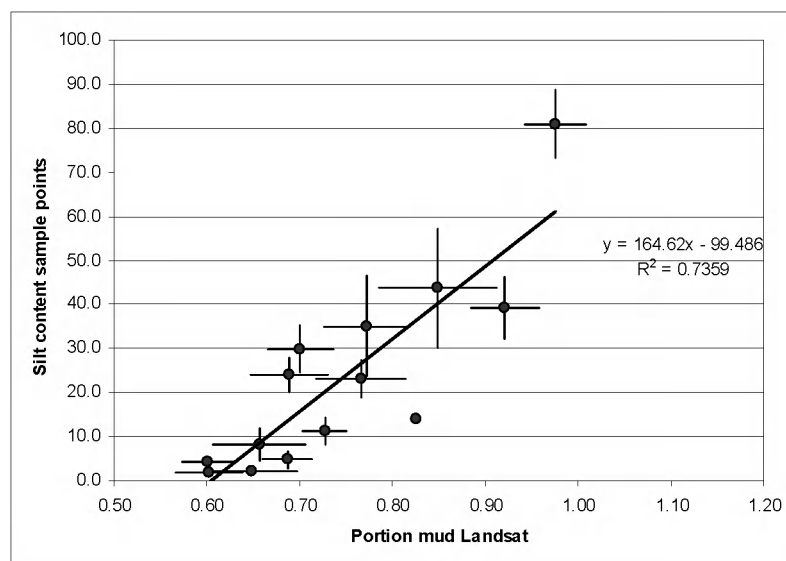
It also has to be taken into account that a satellite pixel represents an area of 30 x 30 meter while the sediment samples only cover a few cm<sup>2</sup>. Intertidal flats can be very inhomogeneous and might not represent the whole area the satellite sees.

The above mentioned possible displacement of the intertidal flat pixels might also cause a problem for the direct pixel to point comparison.

These are reasons why the direct comparison between satellite images and in-situ measurements might be difficult.

#### 4.4.3 Evaluation of the Portion of Dry Mud Endmember

Due to the problems described in the previous section, a solution was needed to improve the comparability of the data sets. As the tendency of the sediments could be found in all results, the intertidal flat areas have been grouped and the average of each group has been calculated. The single "Platen" and "Slikken" have been used in order to group investigation area. The correlation between the two and the resulting regression line is shown in Figure 21. Now a correlation can be detected between the in-situ measurements and the portion of the "dry mud" endmember. However, this method has the disadvantage that the number of points is very much reduced which decreases the statistical significance.



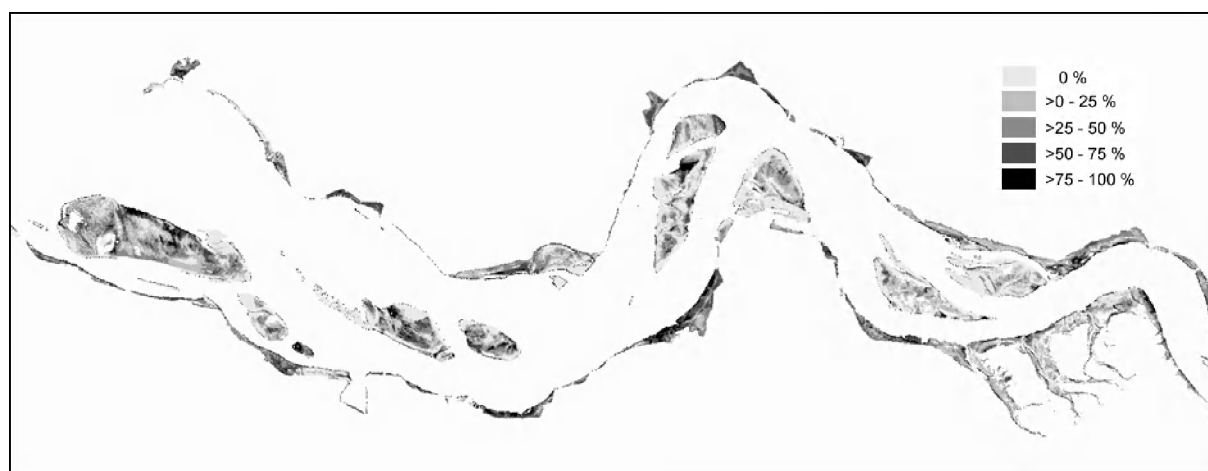
**Figure 21:** Correlation portion of endmember “mud dry” and Silt Content of the sample points (mean of tidal flats, with standard error for each mean value)

#### 4.4.3.1 Results July

The derived formula for the regression

$$y = 164.62 * x - 99.48 \quad [F 6]$$

has been applied to the portion of the dry mud endmember (x) in order to derive the silt content (y) for each pixel. Especially the sandy areas now have negative silt content, this is caused by the averaging of the “Platen” and “Slikken”. But it is obvious, that these areas with negative values are pure sandy areas and therefore, all negative values were set to 0.



**Figure 22:** Silt Content July derived from evaluation of the dry mud proportion to the Silt Content of the in-situ measurements

Figure 23 shows how the descriptive classes of the supervised classification correlate with the silt content derived from the spectral unmixing method.

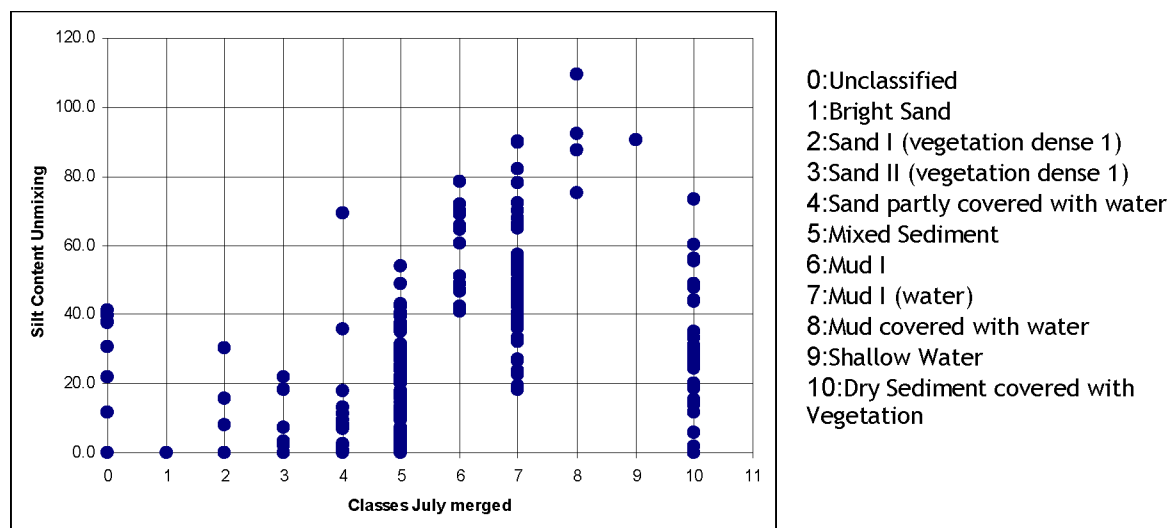


Figure 23: Comparison of Mud content derived from spectral unmixing and Classes of supervised classification (July image, merged trainings set)

#### 4.4.3.2 Results February

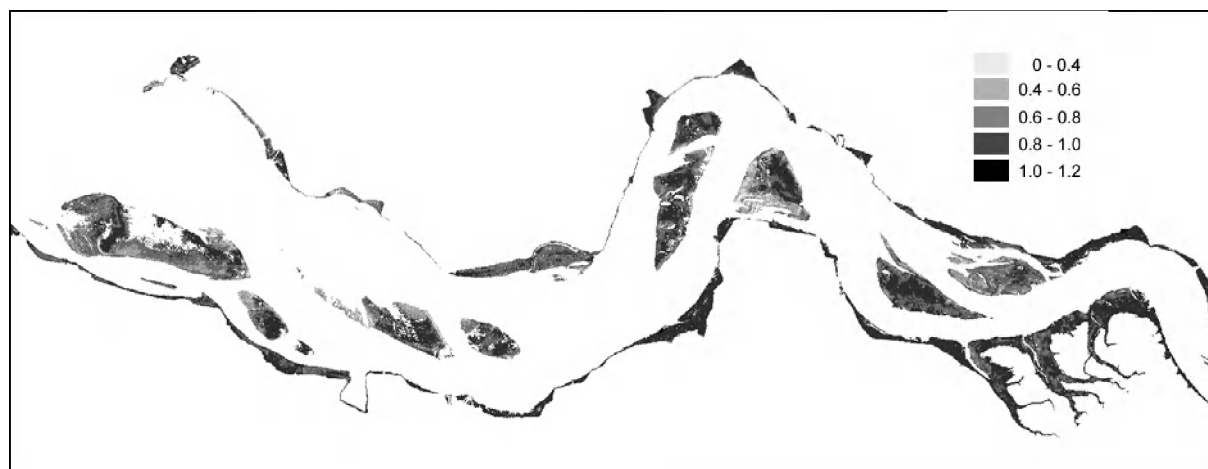


Figure 24: Water corrected portion of dry mud February (without without pixel where the water portion was greater than 0.7 (=70% of the pixel covered by water))

In order to derive the silt content for the February image, the equation found for the July image has been applied. Figure 25 shows the derived silt content.

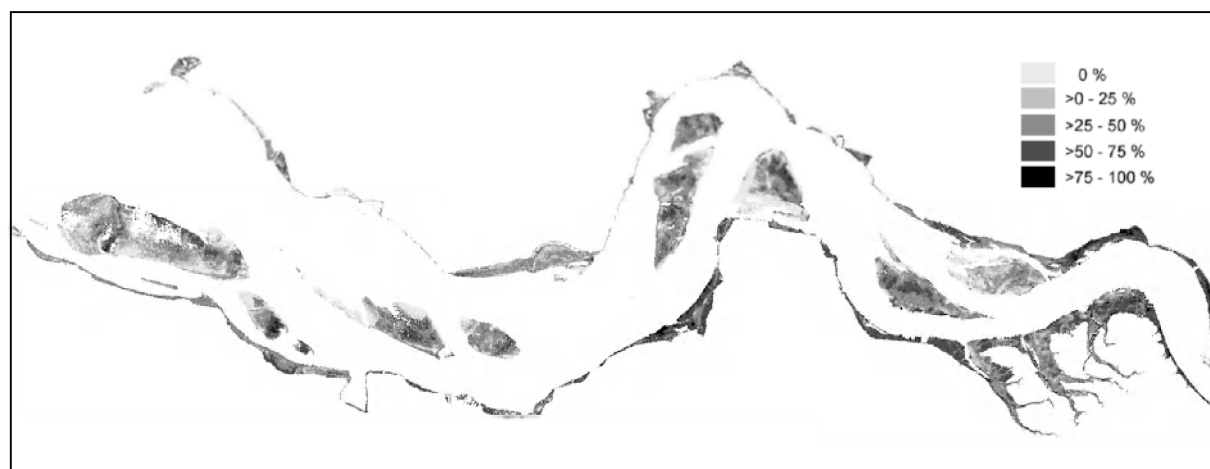


Figure 25: Silt Content February, derived from dry mud portion by applying the regression between in-situ measurements and July image

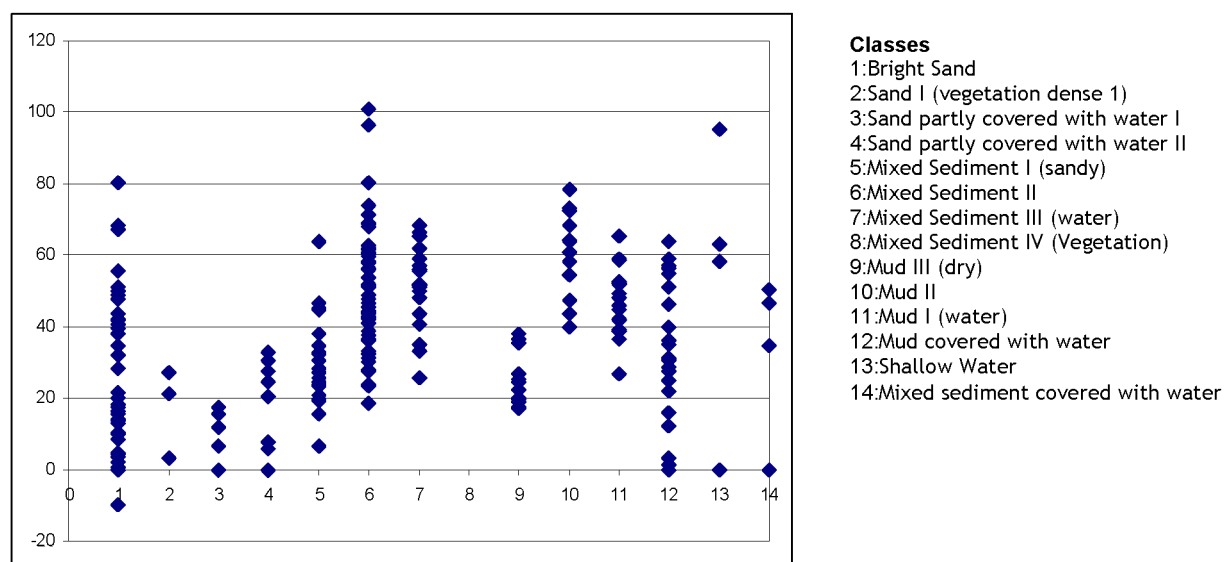


Figure 26: Comparison of silt content derived from spectral unmixing and Classes of supervised classification (February image)

Figure 26 shows how the descriptive classes of the supervised classification correlate with the silt content derived from the spectral unmixing method. It seems that the mud classes, especially the mud (dry) class is more related to mixed sediments. The class “mud covered with water” seems also to include quite sandy pixels, which indicates that the influence of water is still not totally eliminated.

#### 4.4.3.3 Comparison of Silt Content July and February

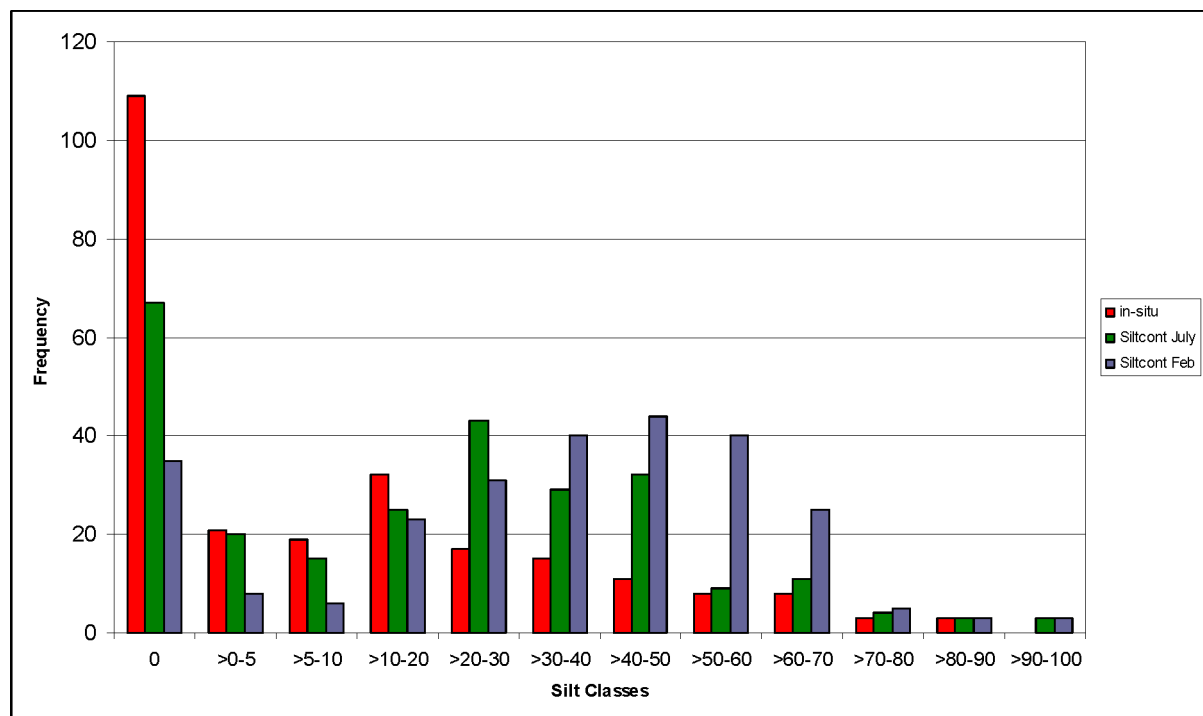


Figure 27: Histogram of silt content of in-situ, July and February image (both derived from linear unmixing method)

The histogram shows that the in-situ measurements have one maximum in the pure sand class (0% silt content) and a secondary maximum in sandy-mixed sediment (>10-20%), while in the July and especially the February image the secondary maximum is shifted to sediment classes with higher silt content (>20-30% for July, 40-50% for February). This indicates that there is an overestimation of mixed and muddy sediments and - as can also be seen in the histogram - an underestimation of pure sand (0% silt content) in the Landsat images compared to the in-situ measurements. The shifting of the July image in comparison with the in-situ measurements might be explainable by the problems explained under section 4.4.2, namely the differences caused by the depth of the samples and the surface seen by the satellite, the spatial representation of the point measurements and the spatial displacement of the georeferenced satellite image. Also errors made by the method can cause an error. Further investigations on this matter on different acquisition times and locations have to be performed for a detailed conclusion. The shifting of the February image in comparison to the July image can be caused by either the method (applying the July regression to the February image due to the lack of in-situ measurements) or can might also be caused by a real change of the upper surface sediments.

#### 4.5 Error Estimation


An important question is how well the satellite data is correlated with the silt content of the top 5 cm of the sediment. Therefore, an error estimation of the regression, used for the calculation of the Silt content from the portion of dry mud derived from linear spectral unmixing, has been performed.

The regression is given by  $y = a \cdot x + b$

$$y = 164.62 \cdot x - 99.48 \quad [F 6]$$

The error for the coefficients  $a$  and  $b$  ( $\Delta a$  and  $\Delta b$ ) is equal to the standard deviation, if the systematic errors can be neglected against the random error.



	<p>Final Report</p>	<p>Doc: SiltCont_report_2.0.doc  Name: Mapping the Silt Content of Westerschelde Sediments using Satellite Data  Date: 19.12.2003  Issue: 1      Revision: <span style="float: right;">Page 26</span></p>
---	---------------------	---

$$\Delta a^2 = S_a^2 = \frac{\sum \Delta y_i^2}{n-2} \cdot \frac{\sum x_i^2}{n \sum x_i^2 - (\sum x_i)^2} \quad [F 7]$$

where

$\Delta y_i$  is the difference between each silt content value ( $y_i$ ) and the calculated value for the regression at position  $x_i$  ( $y_{(x)}$ )  
 $x_i$  is the portion of mud endmember  
 $n$  = number of points taken for calculating the regression

$$\Delta b^2 = S_b^2 = \frac{\sum \Delta y_i^2}{n-2} \cdot \frac{n}{n \sum x_i^2 - (\sum x_i)^2} \quad [F 8]$$

When applying above formulas, the error of the coefficients of the regression are:

$$\Delta a = 21.416$$

$$\Delta b = 16.776$$

The error of an estimated silt content is then

$$\Delta y_i^2 = \left( \frac{\partial y}{\partial a} \right)^2 \cdot \Delta a^2 + \left( \frac{\partial y}{\partial x_i} \right)^2 \cdot \Delta x_i^2 + \left( \frac{\partial y}{\partial b} \right)^2 \cdot \Delta b^2 \quad [F 9]$$

$$\Delta y_i^2 = x_i^2 \cdot \Delta a^2 + a \cdot \Delta x_i^2 + \Delta b^2 \quad [F 10]$$

where

$x_i$  is the portion of dry mud for each pixel  
 $a$  and  $b$  are the coefficient of the regression  
 $\Delta a$  and  $\Delta b$  are the errors of coefficient  $a$  and  $b$   
 $\Delta x_i$  is the RMS error for each pixel calculated with the linear spectral unmixing

This means that the error can be calculated when entering the known values:

$$\Delta y_i^2 = x_i^2 \cdot 21.42^2 + 164.48 \cdot RMS_i^2 + 16.78^2$$

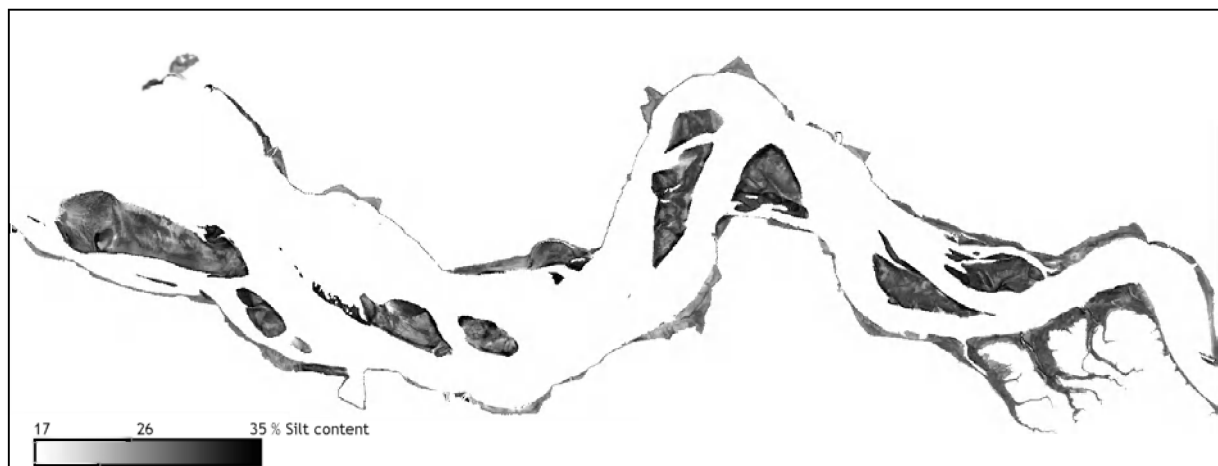


Figure 28: Minimum of absolute error of silt content when applying the regression

Figure 28 shows the minimal possible absolute error of the silt content that can occur when applying the regression derived under section 4.4.3. The absolute error is higher for the muddy areas.

The relative error, that gives the error in percentage of the silt content, can be derived by dividing the absolute error through the silt content itself (see Figure 29).



*Figure 29: Minimum of relative error of silt content*

In this error estimation, it is explicit pointed out that the error that is calculated is the minimum possible error, as there are several error sources that could not be taken into account, e.g. the error of the in-situ measurements or the error caused by the calculation of means for the single tidal flats for retrieving the regression.

#### 4.6 Summary of Results

Two different methods were applied to the satellite data. One delivered concrete sediment type classes, while with the other method a calculation of the silt content was possible. The results of the satellite images seem to be meaningful and both methods give comparable and consistent results.

However it was not possible to retrieve a correlation between the point measurements and the derived silt content at the corresponding pixel in the remote sensing images. This is due to different reasons:

- The transfer of cm<sup>2</sup> in-situ sample data to 30x30 m<sup>2</sup> pixels values
- Differences between the average silt content of 5 cm depths vs. the silt content of the uppermost mm of sediment that can be seen by the satellite
- Georeferencing
- Water coverage of the sediment still may lead to misclassification in the satellite data, although both methods pay great attention to this aspect.


However, the tendency that can be seen in the satellite images and the in-situ measurements could be described by a regression when grouping and averaging the different areas of the Westerschelde.

## 5 Conclusion

From this investigation, the following things can be concluded.

A classification of sediment types and silt content for tidal flats can be derived from satellite data. The knowledge of the area that is investigated is very valuable for the interpretation of the remote sensing data.

When comparing the results retrieved from satellite data and in-situ sediment data, it has to be taken into account that two different measurements, in terms of horizontal extension and vertical integration, are compared. It depends on the question of the application which kind of information and therefore which measurement method is more suitable. The one method is giving a synoptic, spatial overview and distribution of the silt content of the upper surface while the other provides the silt content of an area of a few cm<sup>2</sup> area, also providing information about the underlying sediment type.


	<p>Final Report</p>	<p><b>Doc:</b> SiltCont_report_2.0.doc  <b>Name:</b> Mapping the Silt Content of Westerschelde Sediments using Satellite Data  <b>Date:</b> 19.12.2003  <b>Issue:</b> 1    <b>Revision:</b>    <b>Page</b> 28</p>
---	---------------------	---

Advantage of satellite images;

- Synoptic acquisition (but therefore also strongly dependent on weather conditions at and before the acquisition date)
- Spatial distribution can be detected very well
- Time series of higher frequency possible (due to high effort for field campaigns)

Advantages of point measurements;

- Average of several centimetres and therefore not depending on short-term conditions
- Longer time series available (consistency of methods)

	<p>Final Report</p>	<p><b>Doc:</b> SiltCont_report_2.0.doc  <b>Name:</b> Mapping the Silt Content of Westerschelde Sediments using Satellite Data  <b>Date:</b> 19.12.2003  <b>Issue:</b> 1      <b>Revision:</b> <span style="float: right;">Page 29</span></p>
---	---------------------	--

## 6 Terms of Use

The Landsat-7 TM scenes have been bought by Brockmann Consult (BC) and remain the property of BC. The processed data remain the sole property of BC. RIKZ obtains an unlimited usage of the processed data.

When publishing the results of this investigation, the statement “Data processing by Brockmann Consult 2003” must be added as well as the sentence which Eurimage requires, namely: “Original Data © Landsat 7 ETM, 2002<sup>3</sup>, Distributed by Eurimage”

## 7 Deliverables

- 1 printed map of the silt content for each Landsat image, containing legend etc.
- 1 georeferenced TIFF of silt classes (for use in GIS) for each Landsat image
- 1 report containing all procedural steps and description of results

## 8 Contact

### Technical Contact Person

Kerstin Stelzer  
Tel.: 04152 889 307  
Fax: 04152 889 333  
Email: kerstin.stelzer@brockmann-consult.de

### Administrative Contact Person

Dr. Desmond Murphy  
Tel.: 04152 889 306  
Fax: 04152 889 333  
Email: desmond.murphy@brockmann-consult.de

---

<sup>3</sup> Year of acquisition